26th International Congress on Modelling and Simulation, Adelaide, SA, Australia, 30 Nov–4 Dec 2025
mssanz.org.au/modsim2025

How does bathymetric resolution and mesh design influence estuarine flushing time estimates?

Mojtaba Moravej [a], Paul Branson [b], Matthew Hipsey [c], Casper Boon [c], Daniel Raj David [c], Aditya Singh [d] and Badin Gibbes [a]

[a] School of Civil Engineering, The University of Queensland, St Lucia, Queensland, Australia, [b] CSIRO Environment, Crawley, Western Australia, Australia, [c] Centre for Water and Spatial Science, The University of Western Australia, [d] The Department of the Environment, Tourism, Science and Innovation Queensland Government
Email: m.moravej@uq.edu.au

Abstract: Bathymetry and mesh design are critical to hydrodynamic and biogeochemical modelling of estuaries, yet their influence on transport timescales remains underexplored. We use the Pioneer River estuary, Queensland, to evaluate how bathymetric resolution and mesh generation affect flushing time estimates with the SCHISM model. Three scenarios: low-resolution, high-resolution automated, and high-resolution manually refined were tested under dry, average, and wet flow conditions. Results show that flushing time is sensitive to bathymetric representation, particularly in dry flows. Higher-resolution scenarios produce substantially longer flushing time estimates, with the notable exception of the wet flow scenario in which the longest flushing times associated with the low-resolution bathymetric data. These findings highlight the importance of high-resolution DEMs and automated workflows for realistic estuarine modelling.

Keywords: *hydrodynamic modelling, DEM, SCHISM, tracer, numerical simulation, residence time*

1. INTRODUCTION

The time scale for partial or complete exchange and mixing of estuarine and oceanic waters, often referred to as flushing time, directly influences water quality by controlling the distribution and persistence of nutrients, contaminants, dissolved gases and suspended particles (Dettmann 2001, Josefson and Rasmussen 2000, Monsen et al. 2002, Sanford et al. 1992). Bathymetry is a first-order forcing in coastal domains (Zhang et al. 2024) and therefore has a direct influence on flushing time within estuarine systems, particularly when estimated using numerical models. Consequently, the mesh generation process and the quality of the underlying digital elevation model (DEM) data can play a critical role in determining the simulation outcomes, such as the hydrodynamic, biogeochemical (BGC) behaviour and overall flushing of river-estuary-reef-marine systems.

Traditionally, mesh generation in estuarine and coastal modelling has relied on the modeller's experience. Domain discretisation and the decisions on resolving particular regions of the domain and creating a mesh to get a functioning model have been guided by expert judgement and often influenced by subjective or seemingly arbitrary decisions (Zhang et al. 2024). While this approach can produce workable meshes, its outcomes can vary depending on individual expertise, introduce variability in simulation results, and limit transparency and reproducibility. Zhang et al. (2024) demonstrated that bathymetry quality strongly influences flow, temperature and salinity profiles, stratification, vertical mixing, and local velocities, arguing that bathymetry manipulation, such as smoothing, can introduce biases and systematically alter estuarine behaviour. Similarly, Cai et al. (2022) found that accurately representing complex estuarine geometry was essential for simulating local stratification and water quality variables, particularly hypoxia.

Recent advances have enabled automated workflows for mesh generation (Cassalho et al. , Mani et al. 2021) with associated improvements in transparency and reproducibility of the modelling workflow. It can also enhance efficiency by enabling seamless integration of diverse data sources, for example, combining broad-coverage but low-resolution remotely sensed data with high-resolution yet spatially limited field measurements. It can also facilitate more regular model updates where high-frequency DEM data updates are available. However, the potential implications of automated mesh design on model accuracy, stability, and the representation of key biogeochemical processes remain underexplored in the literature. Therefore, there is a need for systematic comparisons between automated and traditional approaches to better understand their influence on simulation outcomes and to guide best practices in modelling biogeochemical properties of river-estuary-reef systems.

Flushing time is a characteristic transport timescale over which water and dissolved substances are replaced in an estuary through the combined effects of river inflows, tides, and exchange with the coastal ocean. It is often compared with the timescales of biogeochemical processes to calculate mass balances and to understand the dynamics of nutrients and chemical properties (Monsen et al. 2002). Boynton et al. (1995) emphasise its importance, arguing that it should serve as a basis for comparative analyses of ecosystem-scale nutrient budgets. Despite this importance, the sensitivity of flushing time to bathymetric representation has received little attention in the literature, and to the best of our knowledge, has not yet been investigated globally, including for GBR estuaries such as our case study, the Pioneer River Estuary.

Consequently, in this study, we assess the sensitivity of estuarine flushing time to bathymetry quality and mesh generation approaches, using a numerical model to compare low-resolution, high-resolution automated, and high-resolution manually refined meshes.

2. METHODS

2.1. Case study

The case study, the Pioneer River, is located on the central Queensland coast and drains a ~1,577 km² catchment into the Great Barrier Reef Lagoon through the city of Mackay (Figure 1). The headwater streams flow from national parks and state forests into lower reaches dominated by cattle grazing, sugarcane cultivation, and production forestry (Lawrence et al. 2006). The river's flow regime is highly episodic, with most discharge occurring during the summer monsoon (December–April) in one or two major flood events, with peaks typically reaching above 1,500 m^3/s. Annual discharge averages ~900 MCM but varies greatly between years, with floods contributing roughly half the annual flow and most particulate export (Mitchell et al. 2005). From upstream to downstream, the Pioneer River can be subdivided into four distinct sections: Cattle Creek, Upper Pioneer River, Lower Pioneer, and Pioneer River Estuary. The latter section is the focus of our study. The estuary extends upstream to Dumbleton Rocks, just below the Dumbleton Weir, around 14 km from the river mouth (Figure 1). It is influenced by a high tidal range (± 3 m), as well as historical river improvement works such as the construction of upstream Dumbleton weir that limits sediment transport, and rock training walls built to maintain navigation and stabilise banks. The construction of rock training walls, in particular, has played a significant role in the more recent development of the river (Fryar 1999), with the majority of the length of the river within the study area having lined banks.

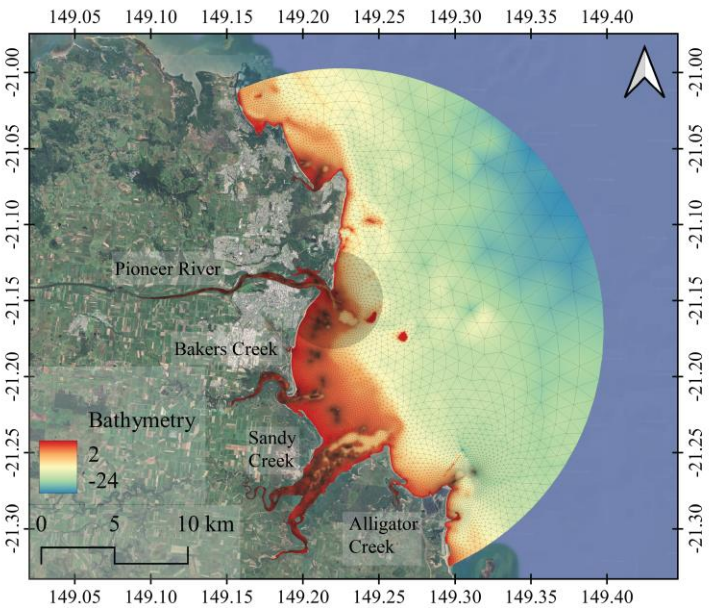

Figure 1. The location of Pioneer River and adjacent minor creek systems (Bakers Creek, Sandy Creek, and Alligator Creek). The figure also depicts mesh and bathymetry used in the high-res scenario (refer to Table 2) and the smaller domain used for e-folding time calculations (shaded grey). Latitude and longitude grid in units of decimal degrees (WGS84 coordinate system, EPSG: 4326), bathymetry values are in meters and referenced to Australian Height Datum (AHD).

2.2. Model setup

We used an open-source community model, the Semi-implicit Cross-scale Hydroscience Integrated System Model (SCHISM), developed by Zhang et al. (2016). SCHISM solves the Boussinesq, primitive equations on a hybrid triangular-quadrangular unstructured grid in the horizontal and hybrid Localised Sigma Coordinates with Shaved

Cells (LSC^2) grid in the vertical (Zhang et al. 2015). We chose SCHISM because its robust, semi-implicit numerical scheme allows testing of different bathymetry qualities, from smoothed to high-resolution unsmoothed DEM, enabling the direct assessment of how bathymetry and mesh quality influence localised hydrodynamic processes and transport timescale estimations. It is acknowledged that part of a typical calibration and validation process for an estuary model involves adjustment of bed friction to match observed flow and water level conditions. Such adjustments are specific to a given set of mesh and bathymetry data. To allow an assessment of bathymetry/mesh resolution on flushing time, independent of the calibration process, we chose to run all models with the same bottom drag coefficient of 0.0025 across the entire domain. Additionally, the Shapiro filter with a numerical smoothing strength of 0.5, with one pass per timestep, was used. No stabilisation method for horizontal viscosity was used (ihorcon = 0).

Simulations are run for 1 month from 01/07/2018 with a time step of 180 s. Atmospheric forcing, including wind, radiation, and precipitation, is sourced from ERA5 (Hersbach et al. 2020) and applied with full spatial and temporal variability. An albedo of 0.06 is applied homogeneously across the domain. The boundary condition includes a constant river inflow depending on dry, average, and wet flow conditions (Table 1) and an ocean boundary. We used 20 years of hourly data from 22/12/2005 00:00 to 9/04/2025 23:00 and quartile classification to estimate the mean flow in dry, average, and wet periods (Table 1). At the open ocean boundary, tidal elevation and velocity are applied using the major constituents M2, S2, N2, K2, K1, O1, P1, and Q1, sourced from the TPXO version 9 global tidal model (Egbert and Erofeeva 2002) interpolated from the nearest TPXO model grids. Salinity of catchment inflows and ocean boundary were set to zero and 34 g/kg, respectively. The model employs a hybrid advection scheme that adapts to local water depth. For depths greater than 5 m, a total variation diminishing (TVD) scheme is used. In shallower regions (< 5 m), a first-order upwind scheme is applied, which, while more diffusive, ensures numerical stability under highly variable wetting and drying conditions. The turbulence closure model is k-kl from Warner et al. (2005). The model was run on the University of Queensland's high-performance computing (HPC) system, Bunya, using 208 CPU cores with 120 GB of memory in total. Each simulation (3 flow conditions × 3 scenarios = 9 runs in total) required between four to six hours to complete.

Table 1. River inflow conditions. Only dry, average, and wet conditions are considered in this study.

Flow condition	Mean inflow (m^3/s)	Range (m^3/s)
Dry (i.e. low flow)	0.61	0.00 – 1.62
Average	5.42	1.62 – 11.71
Wet	100.15	11.72 – 340.09
Extreme wet	793.90	340.10 – 6,329.50

2.3. Scenarios

Three scenarios were developed (Table 2) to evaluate the impact of bathymetric resolution and mesh design on flushing time estimations. For simplicity, the horizontal mesh resolution in the x-y plane is kept constant and is derived to satisfy the High-res+ scenario, but the bathymetry source and its handling are different between scenarios. Horizontally, the mesh consists of 67,762 nodes and 130,884 triangular cells of varying sizes (Figure 1). Vertically, the model is 2D for depth below 0.2 m and gradually has more vertical layers in the deeper regions, up to 22 layers at the 24 m depth (Figure 1). Since the bathymetry data differ among scenarios, the number and distribution of vertical layers are unique to each case, even though the horizontal mesh resolution is fixed.

The High-res model bathymetry was derived from a regional 5 m resolution topography-bathymetry Digital Elevation Model. The DEM combined available Aerial LiDAR point cloud data (https://elevation.fsdf.org.au/) with the Digital Earth Australia (DEA) Intertidal (https://doi.org/10.26186/149403) and Geoscience Australia AusBathyTopo (GBR) 30m offshore (Beaman 2017). The Normalised Difference Water Index (NDWI) was calculated from the "Analysis-Ready" Sentinel 2 MSI satellite data (https://doi.org/10.26186/146552) available on DEA for the 2024 calendar year. A water mask was derived from NDWI > 0 and vectorized using the skeleton-tracing algorithm (https://github.com/LingDong-/skeleton-tracing) to identify creek centrelines. Finally, the creek half-width was calculated from the water mask using the distance_transform_edt function implemented in the python library SciPy. The vectorised creek width information was used to inscribe a channel depth for creek areas based on a power-law relationship:

$$\log(D) = 0.82 * \log(W) - 1.13$$

where D is the creek depth and W is the creek width. This allows for tidal conveyance up into the associated estuaries and floodplains not resolved by the Geoscience Australia AusBathyTopo (GBR) 30m dataset.

The automated mesh generation workflow occasionally produced artefacts where the Aerial LiDAR point cloud data captured bridges and other infrastructure. Most of these artefacts obstructed the main channel and they deemed important in our study because they were altering flow connectivity. So, the artefacts were identified and corrected manually based on observations during the field campaign conducted from 23 to 27 June 2025. The result of these refinements in mesh and bathymetry was High-res+ scenario. An example of such artefacts is presented in Figure 2.

Table 2. Scenario definition

Scenario name	Description
Low-res	Smoothed bathymetry derived from 30 m grids provided by the Geoscience Australia AusBathyTopo (GBR) 30m offshore (Beaman 2017) and a lower resolution compared to the other two scenarios. This scenario represents traditional approaches to mesh generation.
High-res	The High-res scenario incorporates finer-scale bathymetry using an automated mesh generation workflow and captures "out-of-the-box" bathymetric detail of the workflow without any further refinements.
High-res+	It builds on and validates the High-res scenario by manually checking and refining the mesh to remove artefacts and better represent key bathymetric features, especially in the main channel.

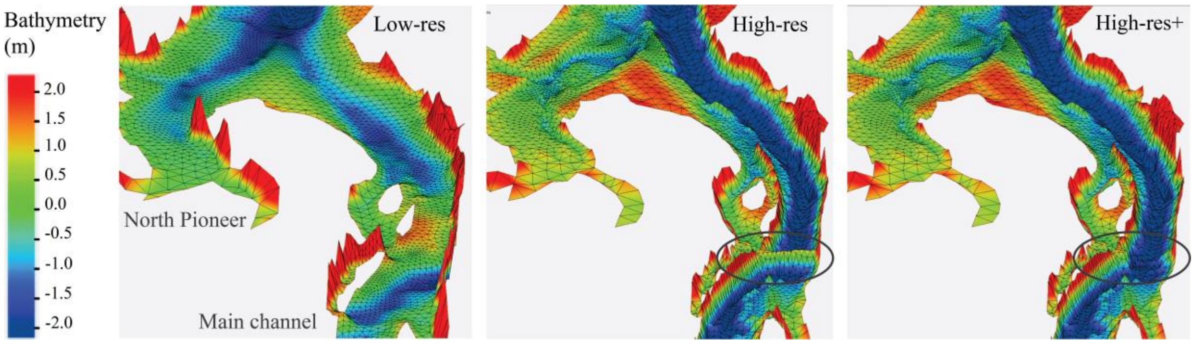

Figure 2. An example of bathymetry representation in the mesh for Low-res (left), High-res (middle), and High-res+ (right) scenarios. Note the artefacts in the main channel in the High-res and refinements made in High-res+ scenario.

2.4. Flushing time

We used the tracer-based Eulerian method described by Taherkhani et al. (2023) to calculate flushing time. In summary, the entire domain was initialised with a passive tracer concentration (c) of 100 kg m^{-3}, while the inflows at the river and ocean boundaries are set to zero concentration. The model is then run to simulate the reduction of tracer concentration due to water exchange. To account for tracer leaving and subsequently re-entering the system via tidal signals, the simulation is run for the entire domain (Figure 1) but the flushing time calculations are performed for the smaller domain (shaded grey in Figure 1), following the suggested method by De Brauwere et al. (2011). Tracer concentrations were averaged across the vertical layers for each water column, and these were subsequently averaged across all horizontal elements to obtain the domain-wide mean tracer concentration for the smaller domain. The domain-wide mean tracer concentration time series, along with the e-folding time (Dettmann 2001), are presented in the results section.

3. RESULTS AND DISCUSSION

Figure 3 shows the reduction of tracer concentration under dry, average, and wet flow conditions for the three bathymetry scenarios (Low-res, High-res, High-res+). In all cases, concentrations decrease approximately exponentially but exhibit strong oscillations driven by tidal exchange. The dashed line corresponds to one e-fold reduction from the initial concentration. Differences between scenarios become most evident in the timing and variability of the reduction, with the low-resolution mesh generally flushing faster and showing less sensitivity to tidal signals, especially in dry and average flows. The High-res and High-res+ scenarios show slower, more oscillatory responses.

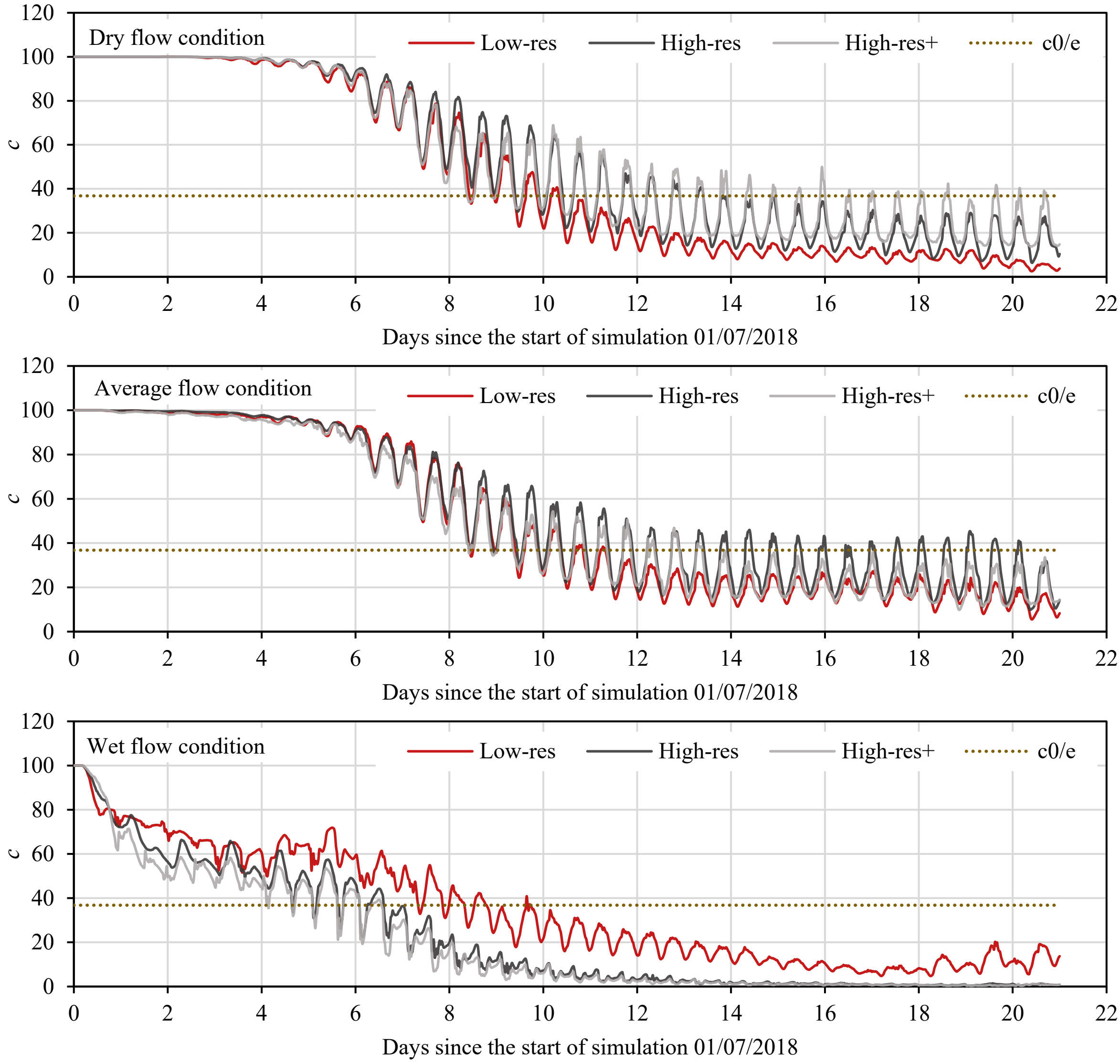

Figure 3. Concentration reduction of passive tracer in Pioneer River under dry, average and flow conditions and three mesh generation scenarios. The c0/e line shows one natural logarithm reduction in concentration.

The e-folding time and re-entry periods for the different flow conditions and mesh scenarios are reported in Table 3. Under dry conditions, all scenarios exhibit similar initial flushing of ~8–9 days. However, the last e-folding time varies significantly, with the High-res+ scenario showing a long re-entry period of around 16 days compared to 3.99 and 1.89 days for the High-res and low-res scenarios, respectively. This suggests that finer bathymetric and mesh detail may be essential for accurately representing the long retention times characteristic of the estuary in dry conditions. In contrast, the Low-res scenario, where the main channel is under-resolved due to smoothed bathymetry, fails to capture the re-entry of the tracer as a response to strong tidal signals (Figure 3). Similarly, the High-res+ scenario, where the representation of the main channel is more detailed compared to the High-res mesh, leads to longer e-folding time and stronger tidal behaviour in dry conditions. The result suggests that even small modifications in the main channel, from High-res to High-res+ scenario, can have a substantial influence on the last e-folding time (increasing from 13.39 to 24.79 days) in dry conditions.

Both High-res and High-res+ have longer e-folding time under average flow conditions. Interestingly, High-res+ shows a shorter last e-folding time (13 days) than High-res scenario under average flow conditions, which differs from the pattern observed under dry conditions. This implies that different interactions between mesh resolution and tidal exchange also depend on the flow conditions. In the High-res+ scenario, better resolution of the main channel and improved connectivity enhanced the influence of river inflow relative to tidal forcing in the average flow conditions, compared with the High-res scenario.

Under wet conditions, the tracer flushes more rapidly in all scenarios, with initial e-folding times around 4–7 days and re-entry periods under 2.5 days. This result is not surprising, as strong river inflow during wet conditions is expected to dominate the hydrodynamics and suppress the re-entry of the tracer via tidal effects. However, it is important to note that the Low-res scenario shows longer e-folding time (Table 3) and the reduction curve consistently sits above other scenarios (Figure 3). This occurs because the smoothed bathymetry in the Low-res mesh under-represents the main channel depth and connectivity; therefore, it reduces conveyance capacity and the effects of strong river inflow during wet conditions. As a result, flushing is less effective compared to the higher-resolution scenarios.

Table 3. e-folding time. initial = first occurrence that concentration dropped below 1/e of initial concentration, last = the last sustained crossing of 1/e threshold, median = midpoint between the two, representing a “typical” flushing time, re-entry period = time between initial and last e-folding time.

Flow condition	Scenario	e-folding time (days since 01/07/2018)			Re-entry period	Percentage change in last e-folding time
		Initial	Last	Median		
Dry	Low-res	8.42	10.31	9.36	1.89	0
	High-res	9.40	13.39	11.39	3.99	29.86
	High-res+	8.38	24.79	16.58	16.42	140.46
Average	Low-res	8.42	11.30	9.86	2.89	0
	High-res	8.92	20.16	14.54	11.25	78.38
	High-res+	8.40	13.37	10.88	4.97	18.24
Wet	Low-res	7.31	9.70	8.50	2.38	0
	High-res	4.63	6.58	5.60	1.95	-32.16
	High-res+	4.13	6.53	5.33	2.41	-32.61

4. CONCLUSIONS

We demonstrated that bathymetric resolution and mesh design strongly influence flushing time estimations in numerical modelling of the Pioneer River, and we infer that these insights also apply to the numerical modelling of other estuaries. Clear differences became evident between the three mesh scenarios. The Low-res scenario, with smoothed bathymetry, generally produced shorter last e-folding time under dry and average conditions and longer e-folding time under wet conditions. It also showed the weakest tidal response and the least tracer re-entry compared to the higher-resolution scenarios. The High-res scenario, where the bathymetry is not smoothed and the main channel is better resolved to enhance connectivity between mesh cells, exhibited stronger tidal influence, with longer flushing times and extended retention relative to Low-res, depending on flow conditions. The e-folding time estimates from the High-res scenario deviated from those of the Low-res scenario by approximately +30%, +78%, and −32% under dry, average, and wet conditions, respectively. The High-res+ scenario, where the representation of the main channel was further refined, produced even longer e-folding times, up to 140% longer compared to the Low-res scenario in dry conditions. These comparisons confirm that flushing time is sensitive to bathymetric representation and mesh design. Under wet conditions, differences between scenarios seem to be smaller as strong river inflows dominate flushing, whereas under dry and average conditions, resolving the main channel and tidal pathways seems to be critical. Flushing time under dry conditions is of particular importance because it represents the most limiting case for water quality and ecological health, and our result showed that it is most sensitive to bathymetry and mesh design. Therefore, we highlight the value of automated mesh generation workflows, the importance of accurately representing key bathymetric features with minimum manipulation of DEM (e.g., smoothing) particularly in the main channel, and the value of high-resolution bathymetry data for achieving realistic model representation of estuarine processes.

ACKNOWLEDGEMENT

Mojtaba Moravej, Badin Gibbes, and Matthew Hipsey acknowledge the funding Queensland Government Department of Environment, Science and Innovation for the Estuarine Modelling Pilot for GBR Catchments research project (2024001895). Paul Branson acknowledges funding by the Australian Government's Reef Trust and CSIRO. This work was supported by resources provided by The University of Queensland Research Computing Centre’s Bunya supercomputer (https://dx.doi.org/10.48610/wf6c-qy55), with funding from The University of Queensland, Brisbane, Australia.

REFERENCES

Beaman, R. (2017) Regional-scale 100/30 m-resolution bathymetry grids for north-eastern Australia.

Boynton, W., Garber, J., Summers, R. and Kemp, W. (1995) Inputs, transformations, and transport of nitrogen and phosphorus in Chesapeake Bay and selected tributaries. Estuaries 18(1), 285-314.

Cai, X., Zhang, Y.J., Shen, J., Wang, H., Wang, Z., Qin, Q. and Ye, F. (2022) A numerical study of hypoxia in Chesapeake Bay using an unstructured grid model: Validation and sensitivity to bathymetry representation. JAWRA Journal of the American Water Resources Association 58(6), 898-921.

Cassalho, F., Mani, S., Ye, F., Zhang, Y. and Moghimi, S. (preprint) Ocsmesh and an End-to-End Workflow for Fully Automatic Mesh Generation with Application to Compound Flood Studies. http://dx.doi.org/10.2139/ssrn.5226658.

De Brauwere, A., De Brye, B., Blaise, S. and Deleersnijder, E. (2011) Residence time, exposure time and connectivity in the Scheldt Estuary. Journal of Marine Systems 84(3-4), 85-95.

Dettmann, E.H. (2001) Effect of water residence time on annual export and denitrification of nitrogen in estuaries: a model analysis. Estuaries 24(4), 481-490.

Egbert, G.D. and Erofeeva, S.Y. (2002) Efficient inverse modeling of barotropic ocean tides. Journal of Atmospheric and Oceanic technology 19(2), 183-204.

Fryar, R. (1999) Pioneer river sand and gravel extraction study, pp. 199-205, National Committee on Coastal and Ocean Engineering, Institution of ….

Hersbach, H., Bell, B., Berrisford, P., Hirahara, S., Horányi, A., Muñoz-Sabater, J., Nicolas, J., Peubey, C., Radu, R. and Schepers, D. (2020) The ERA5 global reanalysis. Quarterly journal of the royal meteorological society 146(730), 1999-2049.

Josefson, A. and Rasmussen, B. (2000) Nutrient retention by benthic macrofaunal biomass of Danish estuaries: importance of nutrient load and residence time. Estuarine, Coastal and Shelf Science 50(2), 205-216.

Lawrence, M.G., Jupiter, S.D. and Kamber, B.S. (2006) Aquatic geochemistry of the rare earth elements and yttrium in the Pioneer River catchment, Australia. Marine and Freshwater Research 57(7), 725-736.

Mani, S., Calzada, J.R., Moghimi, S., Zhang, Y.J., Myers, E. and Pe'eri, S. (2021) OCSMesh: a data-driven automated unstructured mesh generation software for coastal ocean modeling.

Mitchell, C., Brodie, J. and White, I. (2005) Sediments, nutrients and pesticide residues in event flow conditions in streams of the Mackay Whitsunday Region, Australia. Marine Pollution Bulletin 51(1-4), 23-36.

Monsen, N.E., Cloern, J.E., Lucas, L.V. and Monismith, S.G. (2002) A comment on the use of flushing time, residence time, and age as transport time scales. Limnology and oceanography 47(5), 1545-1553.

Sanford, L.P., Boicourt, W.C. and Rives, S.R. (1992) Model for estimating tidal flushing of small embayments. Journal of waterway, port, coastal, and ocean engineering 118(6), 635-654.

Taherkhani, M., Vitousek, S., Walter, R.K., O'Leary, J. and Khodadoust, A.P. (2023) Flushing time variability in a short, low-inflow estuary. Estuarine, Coastal and Shelf Science 284, 108277.

Warner, J.C., Sherwood, C.R., Arango, H.G. and Signell, R.P. (2005) Performance of four turbulence closure models implemented using a generic length scale method. Ocean Modelling 8(1), 81-113.

Zhang, Y.J., Anderson, J., Park, K., Wu, C.H., Wipperfurth, S., Anderson, E., Pe'Eri, S., Beletsky, D., Titze, D. and Di Lorenzo, E. (2024) Debunking common myths in coastal circulation modeling. Ocean Modelling 190, 102401.

Zhang, Y.J., Ateljevich, E., Yu, H.-C., Wu, C.H. and Yu, J.C. (2015) A new vertical coordinate system for a 3D unstructured-grid model. Ocean Modelling 85, 16-31.

Zhang, Y.J., Ye, F., Stanev, E.V. and Grashorn, S. (2016) Seamless cross-scale modeling with SCHISM. Ocean Modelling 102, 64-81.